



Phase transformation and mechanical properties of Ti-(10–30) Zr–3Mo–1Sn alloys

S. Cai^{a,*}, J.E. Schaffer^a, P. Gao^b, X. Wang^c, Y. Ren^d

^a Fort Wayne Metals Research Products Corp, 9609 Ardmore Ave., Fort Wayne, IN, 46809, USA

^b School of Materials Science and Engineering, Shanghai University, Shanghai, 200072, China

^c School of Materials Science and Engineering, Chang'an University, Xi'an, Shaanxi, 710061, China

^d Advanced Photon Source, Argonne National Laboratory, 9700 S. Cass Ave., Argonne, IL, 60439, USA

ARTICLE INFO

Keywords:

Ni-free beta Ti

Super-elasticity

Lattice transformation strain

Synchrotron

Textures

ABSTRACT

Studies on three Ti–xZr–3Mo–1Sn (x=10–30 at.%) alloys found that the influences of Zr on phase transformation and mechanical properties are closely tied to its effect on β -phase stability. It decreases the β -transus by $\sim 8.8^\circ\text{C/at.}\%$, suppresses the formation of α -phase or martensite during cooling and enhances the room temperature super-elasticity. The influence of Zr on lattice transformation strain is weak with the calculated maximum transformation strains of $\sim 8\%$ in all three alloys regardless of their large differences in Zr content. The largest recoverable strain of $\sim 3.8\%$ was obtained in alloy 30Zr after heat treatment at 600°C . Heat treating at 600°C produces a $\alpha+\beta$ dual phase structure with unique texture patterns in alloys 10Zr and 20Zr. Although texture patterns of α and β phases can be understood based on their crystal orientation relationship, mechanisms that caused these textures remain unknown. Aging at 200°C for a short time increases the super-elastic strain without sacrificing material ductility and total recoverable strain.

1. Introduction

Since Ni-related allergic reaction has been reported for implants that are made out of nitinol, a Ni–Ti alloy that shows large super-elasticity at body temperature [1–3], researchers have focused on developing Ni-Free super-elastic beta Ti alloys for years [4–13]. Alloy systems containing one or more β -stabilizers, such as Nb, Mo, V, Cr, Ta and Zr, have been studied [4–31]. By carefully selecting the right amount of these elements, the austenitic β -phase, which has a bcc structure, is retained at room temperature after heat treating, but is able to transform to the α' martensite, which has an orthorhombic structure, during deformation [4]. This Stress-Induced Martensite (SIM) could transform back to austenite upon unloading, which enables the material to recover relatively large deformation strain. This high strain recovery or body temperature super-elasticity is highly demanded for many medical devices. In addition to the β -phase stability, which relies on chemistry, and texture, which is process controlled, this property fundamentally depends on lattice strains associated with the phase transformation. For β -Ti, the maximum phase transformation strain is caused by the $[110]_\beta \rightarrow [010]_{\alpha'}$ transition, which depends on lattice parameters of both phases and is strongly affected by chemical composition. Unfortunately, most of

β -stabilizers have negative effects on phase transformation strain. For example, the transformation strain was found to be decreased by Nb at 0.0034/at.% [4,25], Fe at 0.015/at.% [10], Mo at ~ 0.0089 /at.% [5], Sn at ~ 0.014 /at.% [24] and Ta by ~ 0.003 /at.% [25]. Based on lattice parameters reported for a Ti–17Nb [26] and Ti–17Nb–1Cr [13] alloys, it is estimated that 1 at.% Cr decreases the maximum transformation strain by ~ 0.012 . Most of the β -Ti alloys developed so far have recoverable strains below 4%, much less than that of nitinol [5,8,12–14,18]. To improve the super-elasticity of β -Ti alloys, research should be focused on finding elements that can increase or only cause minimum reduction on transformation strain, while offering effective control of transformation temperatures at the same time. It is also essential that these alloy elements do not jeopardize material strength and ductility. This requires a thorough understanding of influences of alloy elements on phase stabilities, crystal structures and deformation mechanisms in Ti-based alloy systems. This knowledge, however, is still inadequate in spite of many years' studies. As discussed previously [24], the main reason is that influences of each element are likely dependent on others, and only limited chemistry ranges have been studied to date. Further research and data are needed. Our previous studies investigated the effect of Fe [10], Cr [13] and Sn [24] on Ti–Nb based alloys. In this study, we

* Corresponding author.

E-mail address: song.cai@fwmetals.com (S. Cai).

<https://doi.org/10.1016/j.msea.2020.139172>

Received 6 January 2020; Received in revised form 14 February 2020; Accepted 26 February 2020

Available online 29 February 2020

0921-5093/© 2020 Elsevier B.V. All rights reserved.

switched to the Ti–Zr alloy system and focused on influences of Zr on phase stabilities, crystal structures and lattice transformation strains. It is known that Zr stabilizes the β -phase, decreases the martensite transformation temperature by ~ 35 – 42 °C/at.% [12,25,27,28], suppress the ω -phase [29] and increases tensile strength [30]. However, the effect of Zr on transformation strain is controversial. It was found to decrease transformation strain by increasing the lattice parameter of β -phase, but decreasing the b parameter of α'' martensite [12], which could explain the smaller transformation strain of Ti–22Nb–6Zr along the $[110]_\beta$ direction compared to Ti–22Nb [25]. But the same Ti–22Nb–6Zr alloy was also found to have slightly higher transformation strain compared to Ti–22Nb–(2–4)Zr alloys [27], implying an opposite effect of Zr on transformation strain. These authors later suggested that Zr is the best alloying element to replace Nb in increasing the super-elastic strain because the addition of Zr has the same influence on martensite transformation temperature as Nb but has a relatively weaker impact on transformation strain [31]. Indeed, a much higher recoverable strain of $\sim 7\%$ was reported in an equal-atomic Ti–Zr alloy with additional of 1.5Mo and 3Sn [32]. However, in our experience, high Zr containing Ti alloys are prone to oxidization and difficult to process, leading our interest towards relatively lower Zr region for manufacturability. Three alloys with Zr content ranging from 10 to 30 at.% were studied in hopes of finding the trend of its influences, especially on phase transformation strains. Mo and Sn were also added to control the phase transformation temperature in addition to their solid solution strengthening effect [5, 30]. This study provides another set of first-hand data, which further enhances our knowledge on Ti alloys and will be beneficial to both academic research and industrial applications.

2. Materials and experiments

Three Ti alloys with chemical compositions of Ti–10Zr–3Mo–1Sn, Ti–20Zr–3Mo–1Sn and Ti–30Zr–3Mo–1Sn (at.%) were Arc-melted three times from raw elements of greater than 99.8 wt.% purity in argon protective atmosphere and then tilt-casted into $\varnothing 19 \times 100$ mm ingots. These alloys are called “10Zr”, “20Zr” and “30Zr” hereafter. Their oxygen content ranges from ~ 500 to 900 ppm in the as-cast condition. After homogenizing at 1000 °C for 48 h in argon atmosphere, they were extruded at 1000 °C to a diameter of ~ 8.4 mm, then hot swaged at 800 °C to a diameter of ~ 5.6 mm; ground to a diameter of 4.4 mm; and then cold drawn to a diameter of 0.45 mm by traditional wire drawing and annealing processes. The process annealing was carried out at 850–900 °C followed by fast quench in gas. The amount of cold work after the last process anneal was 68% for alloy 10Zr and 50% for alloys 20Zr and 30Zr, respectively. 50% is about the maximum area reduction that can be obtained in alloys 20Zr and 30Zr during cold drawing. Differential Scanning Calorimetry (DSC) testing was carried out to study the martensite transformations between -150 °C and 350 °C. Differential thermal analysis (DTA) testing was used to find out phase transformations, particularly the β -transus, between 20 °C and 950 °C. Cold drawn wires were heat treated at 600–800 °C for 20–30 s in argon and quench to room temperature in 15 s. Heat treated specimens were uniaxially tensile tested through load-unload cycles on an Instron 5966 tensile tester. The sample gauge length was 127 mm. Test was under displacement control at a deformation rate of $1.6 \times 10^{-3} \text{ s}^{-1}$. During the test, specimens were continuously loaded to a strain of 4%, unloaded to zero stress and then re-loaded to fracture.

To understand the influences of heat treating temperature on microstructures and mechanical properties, *ex-situ* synchrotron X-ray diffraction was used to study the phase constitutions of the heat treated and deformed specimens. This experiment was carried out at room temperature on beam line 11-ID-C at the Advanced Photon Source (APS) at Argonne National Laboratory. The wavelength was 0.1173 Å with a sample to detector distance of about 1.5 m. The “raw” data were processed in FIT2D software [33]. Phase fractions and textures were

estimated by Rietveld refinement [34] embedded in the MAUD software [35]. 2D diffraction images were used due to the cylindrical sample geometry. In this case, the 2D image was cut and integrated at 5° azimuth angle (i.e. from -2.5° to 2.5° , 2.5 – 7.5° , etc.) to produce 72 diffraction spectra. These diffraction spectra were then fitted by Rietveld refinement [34] in MAUD software [35]. Examples from alloy 10Zr are given in Fig. 1, which show that experimental results are well captured by Rietveld refinement in both annealed and deformed conditions. Based on these overall good fittings, lattice parameters, crystal orientations and the fractions of different phases can be obtained. More details can be found in some of our previous work [36].

It is known that β -Ti alloys tend to form ω -phase at temperatures between 200 and 500 °C [37], which effectively changes their mechanical properties [5,10]. To investigate the behavior of low temperature aging of these alloys, stress-relieved specimens were heat treated at 200 °C for various amount of time. Higher aging temperature was found to embrittle the material very quickly. Aged specimens were then tensile tested at room temperature. They were first stretched to 6% strain and unloaded to zero stress, heated up to above 200 °C in ~ 5 s, and then re-loaded to fracture. This allows the total recoverable strain,

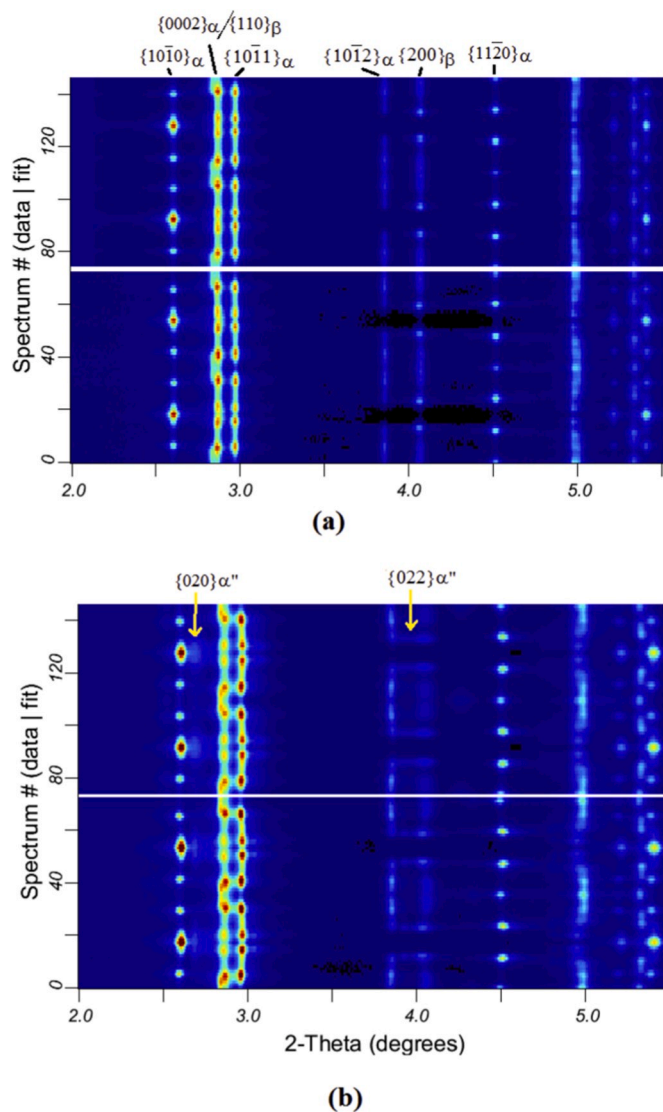


Fig. 1. Comparison between experimental results and modeling results of alloy 10Zr a) after anneal and b) after 4% strain deformation. The upper half of each figure are modeling results and the lower half of each figure are experimental data.

including both super-elastic and shape memory strains, to be measured.

3. Results and discussions

3.1. Microstructures and phase transformation

Fig. 2 shows microstructures of different alloys at room temperature after process anneal (i.e. 900 °C for 10Zr and 850 °C for 20 and 30Zr). It can be seen that while 20Zr and 30Zr have an equi-axed single β -phase microstructure, 10Zr shows a lath-like microstructure inside the original β -grains, suggesting that the high temperature β -phase has transformed to martensite phase after quench to room temperature. Phase constitutions after heat treatment at different temperatures are further revealed by synchrotron x-ray as shown in Fig. 3. For 10Zr, heat treating at 600 °C produced α and β dual phase structure (Fig. 3 a), with volume fractions of \sim 79.6% and 20.4% respectively based on Rietveld refinement. The amount of α -phase was decreased with increasing heat treatment temperature. At 700 °C, the volume fraction of α -phase was decreased to \sim 60% (Fig. 3b). Finally, after heat treated at 800 °C and quench to room temperature, martensite phase dominated with a very small amount of residual β -phase (Fig. 3c). It is worth mentioning that this thermal martensite has an orthorhombic crystal structure, which is the same as that of SIM. This is different from the *hcp* crystal structure of the thermal martensite found in a Ti-15 wt.%Zr alloy [38]. No ω -phase was detected in this alloy. For 20Zr, there were about 50% α and 50% β phases after heat treatment at 600 °C (Fig. 3d). However, after heat treatment at 700 °C, α -phase disappeared and there was \sim 8% ω -phase in addition to the majority of β -phase (Fig. 3e). In comparison, alloy 30Zr consisted of large amount of β -phase and \sim 10% ω -phase after heat treatment at temperatures from 600 to 800 °C (Fig. 3f). These results suggest that the β -transus is somewhere between 700 and 800 °C for 10Zr, between 600 and 700 °C for 20Zr and below 600 °C for 30Zr. This is confirmed by the DTA testing. Fig. 4 shows that β -transus measured by DTA is \sim 766, 680 and 590 °C for 10Zr, 20Zr and 30Zr respectively. It is estimated that Zr decreases the β -transus by \sim 8.8 °C per atomic percentage in Ti–Zr–Mo–Sn system. However, repeated DSC tests were not able to detect martensite phase transformation in all three alloys. Lattice parameters of different phases in different alloys are listed in Table 1. Adding Zr content expands the bcc β phase volume.

Fig. 5 shows the inverse pole figures of α and β phases of alloy 10Zr after heat treatment at 700 °C. α -phase has a strong fiber texture spreading from $\{10\bar{1}0\}_{\alpha}$ to $\{30\bar{3}1\}_{\alpha}$. β -phase has a weaker texture band ranging from $\{113\}_{\beta}$ to $\{214\}_{\beta}$. This β -phase texture is new and will be discussed later. Texture patterns in other two alloys are similar to those found in Ti–17Nb–1Fe [10] and thus are not repeated here.

3.2. Mechanical properties

Fig. 6 shows the tensile stress-strain curves of different alloys after heat treatment at temperatures from 600 to 800 °C. After heat treatment at 600 °C, both 10Zr and 20Zr exhibited a brittle behavior. They fractured at a stress of \sim 1.4 GPa with very limited plastic deformation. While the ductility of both alloys quickly increased and their strength quickly decreased with increasing the heat treatment temperature, their deformation responses are very different after heat treatment at temperatures above 700 °C (Fig. 6a and b). 10Zr showed typical elastic-plastic deformation behavior. On the other hand, “double yielding” was observed on 20Zr. After a short elastic deformation, the material yielded at stresses close to 200 MPa and then showed a plateau region, where the stress kept almost a constant with increasing strain due to SIM transformation. A second elastic region was seen between \sim 3 and \sim 8% strain, and then yielded at stresses of \sim 1000 MPa. Not too much strain was recovered after unloading at 4% strain, indicating that the SIM was mostly stable at room temperature. In comparison, 30Zr was less strong but more ductile after heat treatment at 600 °C. Most importantly, it showed a super-elastic behavior (Fig. 6c). After apparent yield at a stress slightly above 400 MPa, deformation entered a plateau region. Upon unloading, this material was able to recover almost all of the 4% deformation strain with a permanent strain \sim 0.14%. The yield strength during the re-loading cycle, \sim 250 MPa, is much less than that of the first loading, which can be attributed to residual martensite giving easy martensite variant path selection. After yield, the stress continued to increase with fracture at 1052 MPa when the deformation strain reached \sim 13.7%. Increasing heat treatment temperature decreased the yield strength, tensile strength as well as the strain recovery. Detailed mechanical properties of these alloys heat treated at different temperatures are listed in Table 2. Clearly, increasing Zr content decreases the tensile strength regardless of the heat treatment temperature. Yield strength and Young's modulus followed the same trend when heat treated at 600 °C. After treatment at higher temperatures, the lowest yield strength and modulus was found in alloy 20Zr followed by 30Zr and then 10Zr.

3.3. SIM phase transformation

SIM can be seen in all three alloys after deformation (Fig. 7). These samples were all heat treated at 700 °C. Therefore, the sample of 10Zr had a α + β dual phase structure before deformation (Figs. 1a and 3b). Clearly, β -phase in this alloy was not stable and transformed to martensite during deformation and the material consisted of α , β and α' phases after unloading from 4% strain. There were about 26% residual α' -martensite based on Rietveld refinement (Fig. 1b). For 20Zr and 30Zr, unloading from 4% deformation left \sim 68% and 32% α' -martensite

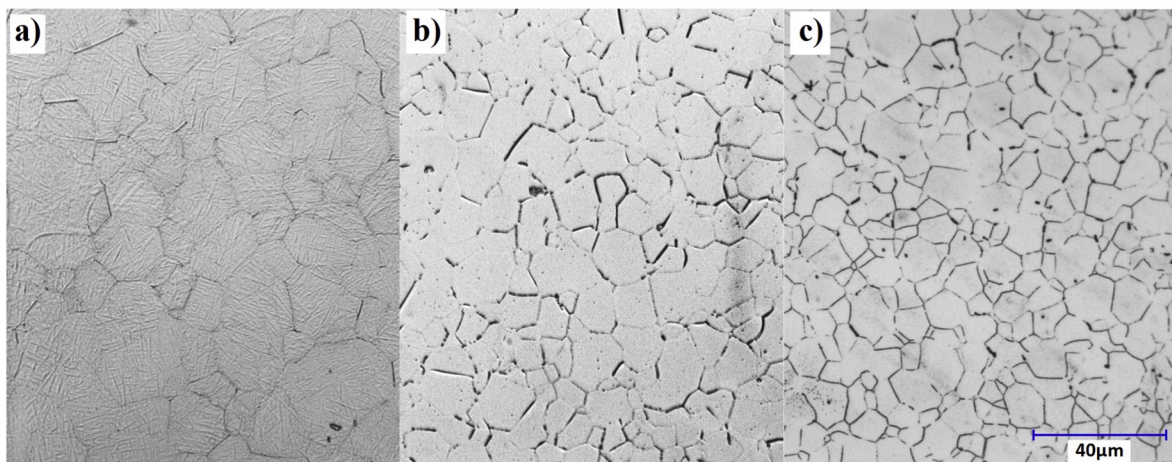


Fig. 2. Microstructure of alloys a) 10Zr, b) 20Zr and c) 30Zr after process anneal.

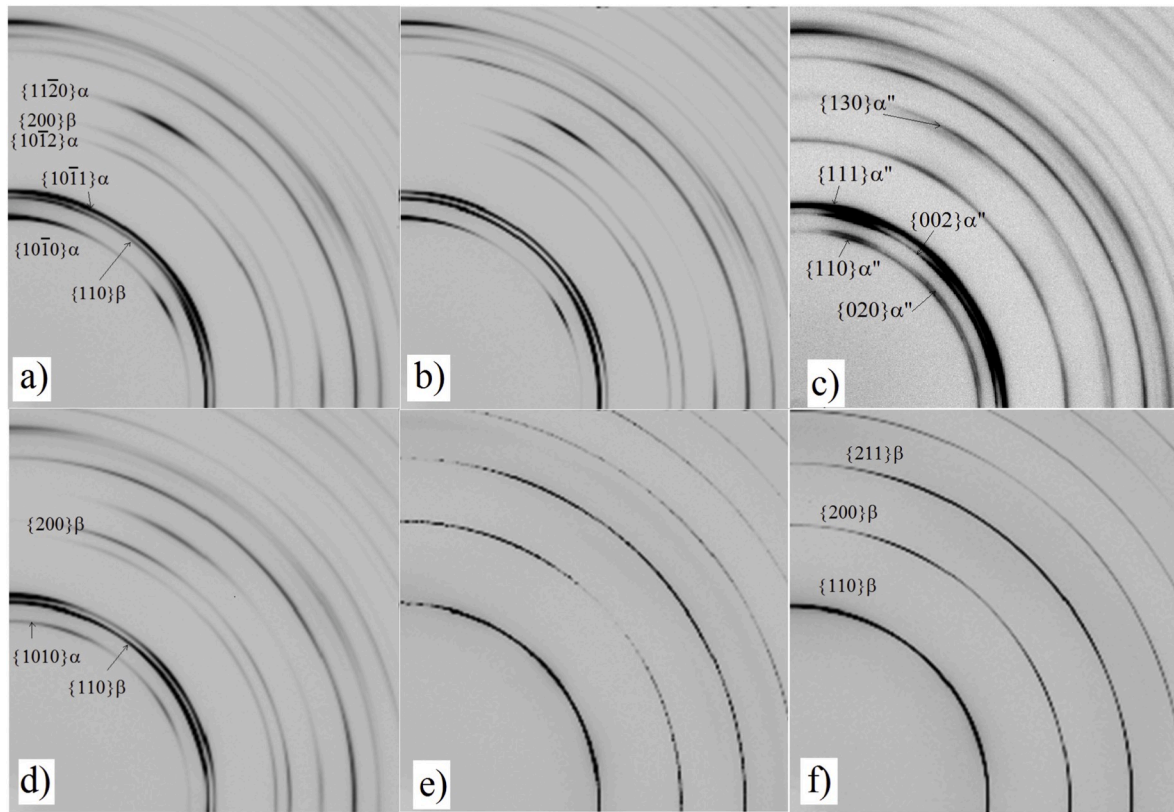


Fig. 3. Diffraction images of alloy 10Zr annealed at 600 °C, 700 °C, 800 °C (a–c); alloy 20Zr annealed at 600 °C, 700 °C (d–e) and alloy 30Zr annealed at 600 °C (f).

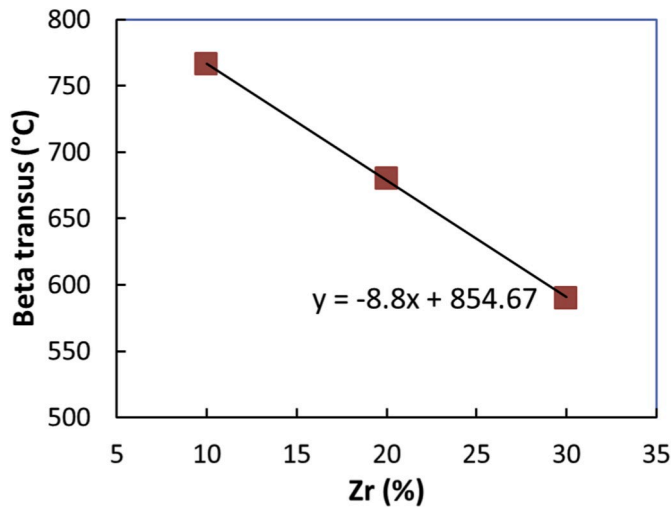


Fig. 4. Influence of Zr on β -transus.

along with the residual β and ω phases. Lattice parameters of SIM phases in these alloys are listed in Table 1 and are also plotted in Fig. 8. It can be seen that increasing Zr content slightly decreases the α -parameter, but

increases the b and c parameters of SIM. The maximum phase transformation strains of these alloys can be calculated along the $[110]_{\beta} \rightarrow [010]_{\alpha'}$ transition [4]. It shows that the maximum transformation strain was only slightly changed from $\sim 7.5\%$ to $\sim 8\%$ from 10Zr to 30Zr (Fig. 8), confirming the weak effect of Zr that was previously reported by others [31]. These transformation strains, however, are much larger compared to those found in other β -Ti alloys [4,10,13].

3.4. Effect of aging

The main goal of this section is to investigate the influence of aging on strain recovery of β -Ti alloys. Since early studies have shown that the majority of 10Zr is α -phase, only 20Zr and 30Zr were investigated here. Stress-strain curves of aged samples are illustrated in Fig. 9, and changes in mechanical properties with aging time up to 60 min are shown in Fig. 10. It can be seen that, for both alloys, aging at 200 °C increased the yield stress and Young's modulus, but had limited influences on ultimate tensile stress and elongation. For 20Zr, aging didn't significantly change the super-elastic strain (i.e. strain recovery upon unloading) and shape memory strain (i.e. strain recovery by heating- Rs). However, for alloy 30Zr, its super-elastic strain was clearly increased and shape memory strain was decreased by aging treatment. Nevertheless, the effect of aging on the total strain recovery, R , of both alloys is small. The maximum total strain recovery measured after 6% strain deformation is $\sim 5.2\%$ and 5.4% for 20Zr and 30Zr respectively.

Table 1

Lattice parameters (Å) of phases in different alloys. Materials were annealed at 700 °C. Lattice parameters of martensite, α'' , are measured from the deformed samples.

Alloy	α		β	ω		α''		
	a	c	a	a	c	a	b	c
10Zr	2.981	4.729	3.311			3.147	5.041	4.737
20Zr			3.343	4.646	2.913	3.091	5.089	4.748
30Zr			3.389	4.889	3.000	3.108	5.177	4.789

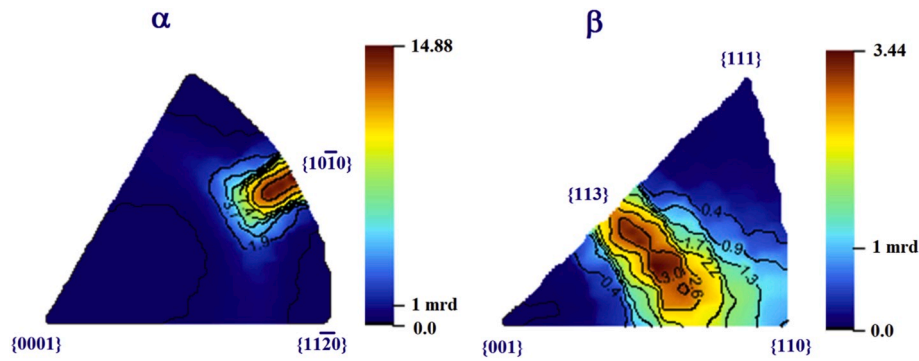


Fig. 5. Inverse pole figures of α and β phases of alloy 10Zr after heat treatment at 700 °C.

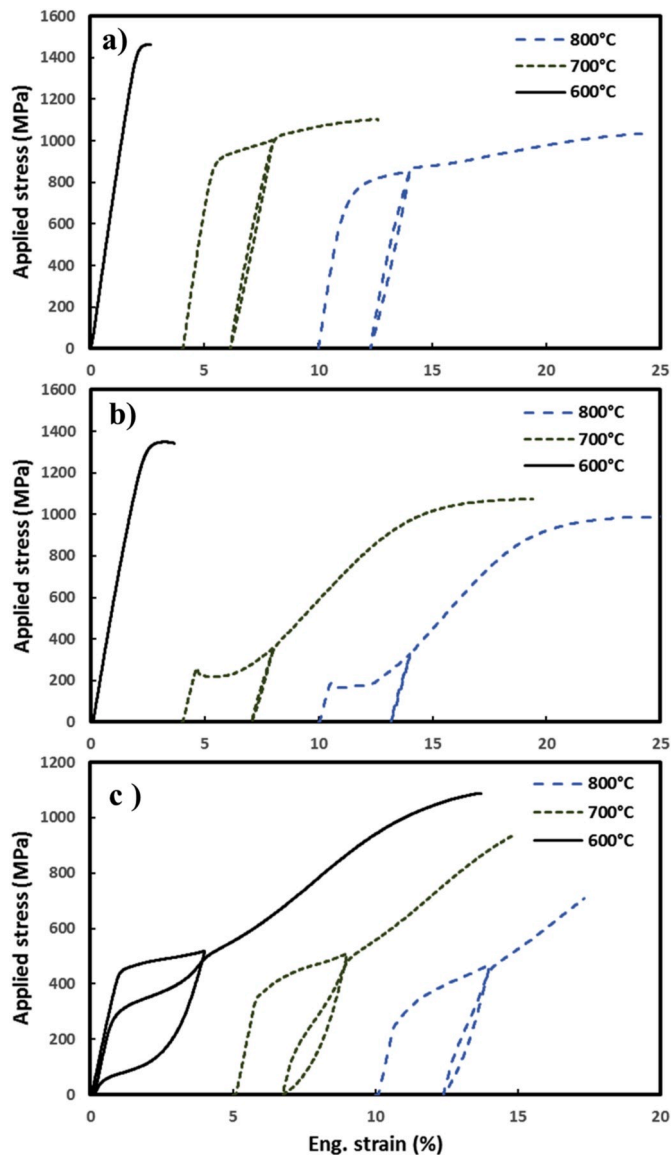


Fig. 6. Stress-strain curves of a) 10Zr, b) 20Zr and c) 30Zr heat treated at different temperatures for 30 s.

Since all three alloys have similar β -grain sizes after the same heat treatment, thus it is reasonable to believe that the change of Zr content only caused negligible contribution in grain-boundary strengthening effect. Clearly, influences of Zr on microstructures and mechanical

Table 2

Mechanical properties of different alloys after heat treatment at different temperatures.

Alloy	Temp. (°C)	$\sigma_{0.2}$ (MPa)	UTS (MPa)	E (GPa)	e% (Perm. Set)	Perm. Set (%)
10Zr	600	1419.3	1463.6	78.7	2.7	
	700	846.9	1071	72.8	8.6	2.1
	800	644.2	1016.3	70.0	14.3	2.3
20Zr	600	1189.9	1388	66.8	3.7	
	700	231.5	1053.5	46.4	15.5	3.0
	800	171.6	977.7	44.1	15.8	3.1
30Zr	600	436.3	1052.7	47.9	13.7	0.14
	700	349.7	891.6	48.6	13.2	1.67
	800	279.1	704.8	47.3	7.3	2.3

properties are closely tied to its effect on β -phase stability. Increasing Zr content stabilizes β -phase and pushes phase transformation to a lower temperature range, which makes 10Zr and 20Zr more prone to form α -phase compared to 30Zr. For 10Zr heat treated at 600–700 °C and 20Zr heat treated at 600 °C, part of their high strength is likely due to the presence of α -phase. In addition to α -precipitate hardening, the formation of α -phase pushes β -stabilizers towards the residual β matrix, which increases its stability and leads to higher transformation stress. α -phase is also responsible for the higher Young's modulus of 10Zr and 20Zr heat treated at 600 °C. Without α -phase, the yield strength of these alloys depends primarily on their β -phase stability. The lower the β -stability, the lower the critical stress for SIM. This explains the lower yield strength of 20Zr compared to 30Zr after heat treating at temperatures above 700 °C. Lower β -stability of 20Zr also made the reverse $\alpha'' \rightarrow \beta$ transformation more difficult and left the most residual SIM at room temperature after unloading. Therefore, no obvious super-elasticity was seen in this alloy (Fig. 6b). For 30Zr, the critical stress for SIM and the super-elastic strain were both decreased with increasing annealing temperature (Fig. 6c), meaning that the β -phase stability were increased by residual cold work. Similar effects of residual cold work have been reported in other β -Ti alloys [40] and NiTi alloys [41]. Residual cold work also increases critical stresses for dislocation or twinning, thus preventing permanent deformation and increasing the total recoverable strain [4]. Age hardening has a similar effect on increasing recoverable strain [4]. In addition, formation of β -stabilizer-lean phases (e.g. ω phase) during aging pushes more β -stabilizers into matrix and enhances super-elasticity [42]. For our case, it appears that the major contribution of aging is from the change of matrix chemistry composition rather than precipitate hardening. Therefore, although the critical stress for SIM transformation and super-elastic strain were increased, tensile strength and elongation were not affected. Since the strength of material was not significantly changed, thus the total recoverable strain and plastic strain were not affected by aging. It is worth mentioning that, despite the large difference in Zr content, the total recoverable strains of 20Zr and 30Zr

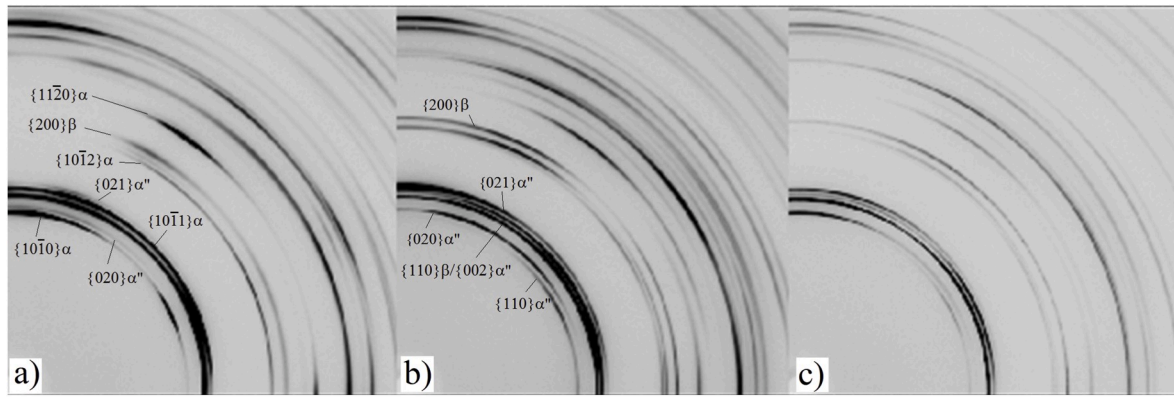


Fig. 7. X-ray diffraction image of a) 10Zr, b) 20Zr and c) 30Zr after deformation. All samples were heat treated at 700 °C for 30 s before deformation.

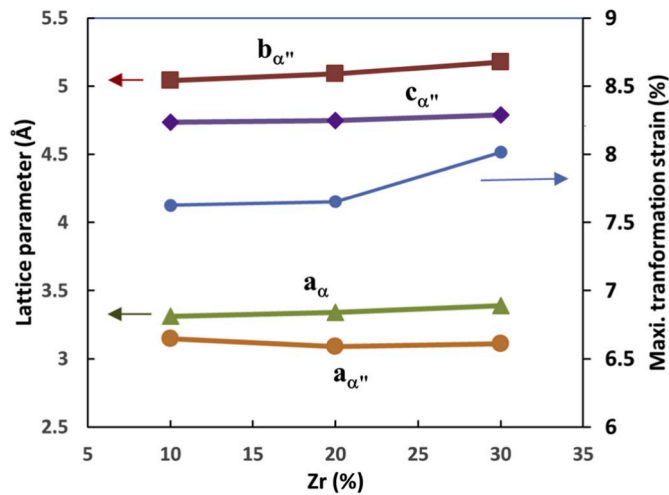


Fig. 8. Effect of Zr on lattice parameters of β and α'' phase and maximum phase transformation strains.

are very close (Fig. 10b). These values (i.e. $\sim 5.2\%$ and 5.4% at 6% deformation strain) are lower compared to the calculated maximum lattice transformation strains. The weak $\{210\}_\beta$ texture observed in these alloy basically makes the maximum transformation strain, which happens in $\langle 110 \rangle_\beta$ direction, impossible. The plastic deformation associated with SIM also prevents it from full recovery, thus limiting the total recoverable strain. Nevertheless, the $\sim 5\%$ total recoverable strain and the $\sim 8\%$ maximum transformation strain of these alloys are

encouraging and Ti–Zr alloy systems appear promising by this measure of performance. Further work includes optimizing chemistry and processing to enhance the strength of $\{110\}_\beta$ texture component and to increase the strength of the matrix to minimize the plastic deformation during SIM transformation.

While the $\{10\bar{1}0\}_\alpha$ fiber texture of 10Zr is typical for extruded rods of hexagonal metals [39], the $\{211\}_\beta$ to $\{421\}_\beta$ texture band of β -phase is new and different from the $\{210\}_\beta$ texture often seen in meta-stable β -Ti alloys [10,13]. However, texture patterns in α and β phases are closely related to each other and follow their crystal orientation relationships during phase transformation. From Fig. 11, it can be seen that α and β phases have a relationship of: $[100]_\alpha \rightarrow [100]_\beta$, $[010]_\alpha \rightarrow [\bar{1}1\bar{1}]_\beta$ and $[001]_\alpha \rightarrow [011]_\beta$. Therefore, the lattice transformation between α -phase and β -phase can be expressed as:

$$[UVW]_\beta = [UVW]_\alpha \times \begin{Bmatrix} 1 & 0 & 0 \\ -0.5 & 0.5 & -0.5 \\ 0 & 1 & 1 \end{Bmatrix} \quad (1)$$

Here, the crystal direction of the *hcp* α -phase is in the form of $[UVW]_\alpha$ instead of $[uvw]_\alpha$. Based on this equation, plane-normal of some of the $\{10\bar{1}0\}_\alpha$ families are actually parallel to the $\langle 311 \rangle_\beta$ direction. For example, plane-normal of $(10\bar{1}0)_\alpha$, $(1\bar{1}00)_\alpha$ and $(\bar{1}010)_\alpha$ are $[210]_\alpha$, $[1\bar{1}0]_\alpha$ and $[2\bar{1}0]_\alpha$ directions. They can be converted to $[31\bar{1}]_\beta$, $[3\bar{1}1]_\beta$ and $[\bar{3}1\bar{1}]_\beta$ directions based on the above equation. Similarly, the $(\bar{3}301)_\alpha$ plane normal (i.e. $[\bar{2}.25, 2.25, 0.447]_\alpha$ direction) is aligned in the $[1.57, 0.68, 3.37]_\beta$ direction, which is only $\sim 2.6^\circ$ away from the $[214]_\beta$ direction calculated using lattice parameters listed in Table 1. Therefore, it is reasonable to believe that the $\{10\bar{1}0\}_\alpha$ to $\{30\bar{3}1\}_\alpha$ textures of

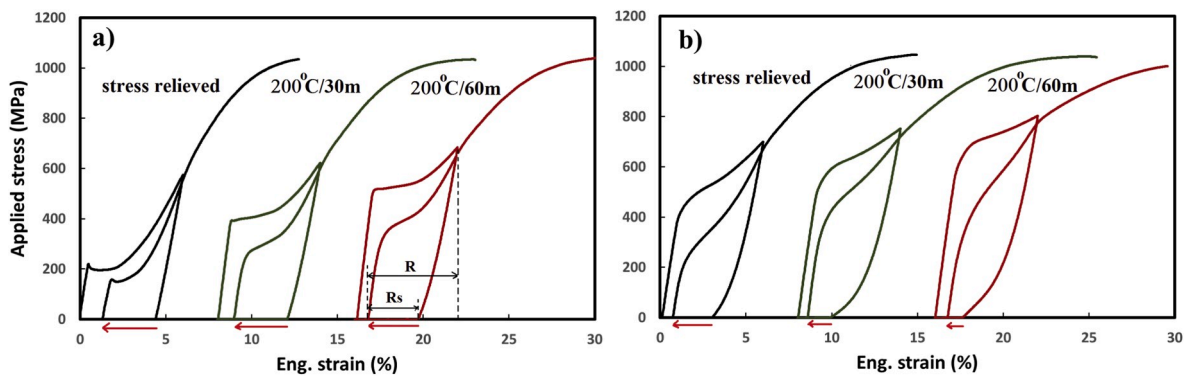


Fig. 9. Stress strain curves of a) alloy 20Zr and b) 30Zr after aging for different amount of time. Samples were stress-relieved at 700 °C for 20 s before aging. Red arrows show the strain recovery, R_s , upon heating after unloading. R is the total strain recovery. (For interpretation of the references to colour in this figure legend, the reader is referred to the Web version of this article.)

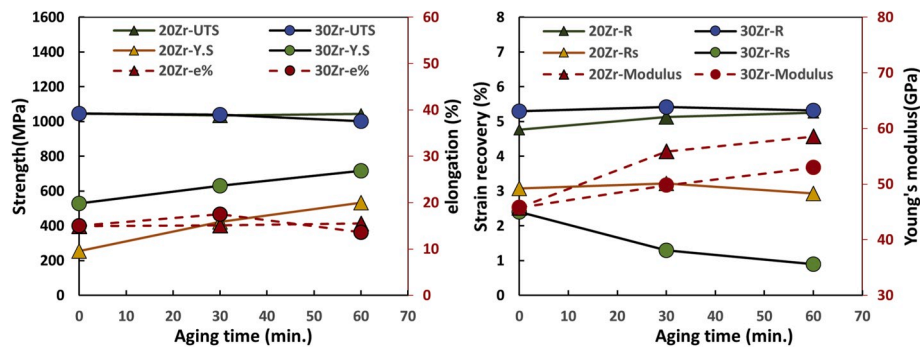
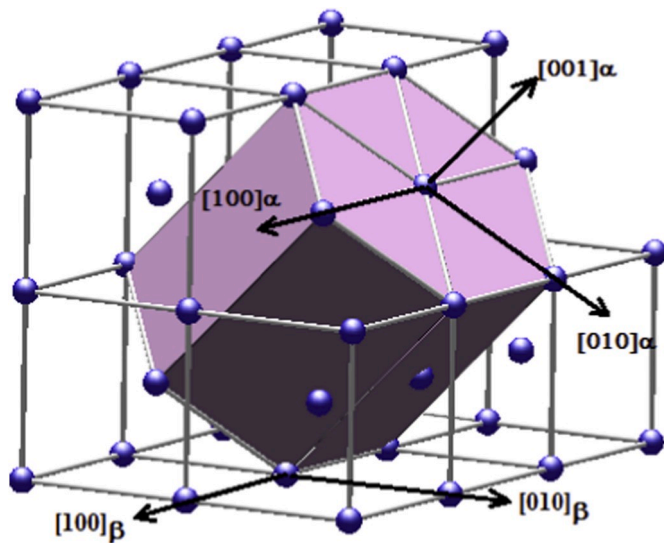


Fig. 10. Influence of aging on mechanical properties.

Fig. 11. Crystal orientation relationship between α and β phases.

α -phase were formed from the $\{113\}_{\beta}$ to $\{214\}_{\beta}$ β -texture band during heat treatment. It is worth noting that, in addition to $\{10\bar{1}0\}_{\alpha}$ family, the $\{113\}_{\beta}$ family could also transform to other α -phase families. For example, $[311]_{\beta} \rightarrow [301]_{\alpha} \rightarrow (2\bar{1}\bar{1}1)_{\alpha}$ and $[131]_{\beta} \rightarrow [111]_{\alpha} \rightarrow (11\bar{2}3)_{\alpha}$. It is not clear why only $\{10\bar{1}0\}_{\alpha}$ family was preferred by phase transformation. According to lattice parameters, d -spacing of $\{10\bar{1}0\}_{\alpha}$ family (i.e. 5.16 Å) is between those of $\{2\bar{1}\bar{1}1\}_{\alpha}$ and $\{11\bar{2}3\}_{\alpha}$ families (~ 5.06 Å and 5.59 Å, respectively). Thus the lattice strain associated with the phase transformation may not play the dominant role on variant selection during cooling. Also it is not known how this special β -phase texture was developed during process. As we have learned so far, the phase constitution in alloy 10Zr can be significantly affected by processing history. It could consist of different amount of β , α and α' phases depending on the heat treatment temperature, cooling rate and cold work level. Each phase has its unique deformation systems and will develop different texture during cold forming, which ultimately affects textures at finish. To fully explain the texture development in this alloy, one needs to trace back to the beginning of the processing and understand the influences of each processing step. These questions, although interesting, are outside the scope of the current project and need to be studied in the future.

4. Conclusions

Three Ti–Zr–Mo–Sn alloys with Zr content from 10 to 30 at.% were studied. It is found that influences of Zr on phase transformation and mechanical properties are closely tied to its effect of increasing the

β -phase stability. Zr decreases the β -transus by ~ 8.8 °C/at.% and suppresses the formation of α -phase or martensite during cooling and enhances the room temperature super-elastic behavior during deformation. However, the influence of Zr on lattice transformation strain is weak. All three alloys have the calculated maximum transformation strains of ~ 7.5 –8%. After 4% strain deformation, the largest room temperature recoverable strain of $\sim 3.8\%$ was obtained in alloy 30Zr after heat treatment at 600 °C. Heat treating at 600 °C produces a $\alpha + \beta$ dual phase structure with unique texture patterns in 10Zr and 20Zr. Although texture patterns of α and β phases can be understood based on their crystal orientation relationship, mechanisms that caused these textures remain unknown. For certain conditions, aging at 200 °C can be used to improve the super-elastic strain of β -alloys without significantly damaging the ductility and total recoverable strain performance.

Data availability

The raw data required to reproduce these findings are available to download from <https://doi.org/10.17632/gr96gshf5p.1>. The processed data required to reproduce these findings are available to download from <https://doi.org/10.17632/gr96gshf5p.1>.

Declaration of competing interest

No conflict of interest exists.

CRediT authorship contribution statement

S. Cai: Writing - original draft, Conceptualization, Investigation, Methodology, Formal analysis. **J.E. Schaffer:** Conceptualization, Writing - review & editing. **P. Gao:** Investigation, Visualization. **X. Wang:** Investigation, Methodology. **Y. Ren:** Writing - review & editing.

Acknowledgement

This study was funded by Fort Wayne Metals Research Products Corp. This research used resources of the Advanced Photon Source, a U. S. Department of Energy (DOE) Office of Science User Facility operated for the DOE Office of Science by Argonne National Laboratory under Contract No. DE-AC02-06CH11357. Data were analyzed by using FIT2D, Maud and GSAS software.

References

- [1] Z. Jia, J. Tu, K. Wang, G. Jiang, W. Wang, J. Vasc. Intervent. Radiol. 26 (2015) 1375–1377.
- [2] P. Jetty, S. Jayaram, J. Veinot, M. Pratt, J. Vasc. Surg. 58 (2013) 1388–1390.
- [3] E. McLucas, Y. Rochev, W.M. Carroll, T.J. Smith, J. Mater. Sci. Mater. Med. 19 (2008) 975–980.
- [4] H.Y. Kim, Y. Ikehara, J.I. Kim, H. Hosoda, S. Miyazaki, Acta Mater. 54 (2006) 2419–2429.
- [5] Y. Al-Zain, H.Y. Kim, H. Hosoda, T.H. Nam, S. Miyazaki, Acta Mater. 58 (2010) 4212–4223.

- [6] X.H. Min, S. Emura, L. Zhang, K. Tsuzaki, *Mater Sci Eng A* 497 (2008) 74–78.
- [7] S. Ishiyama, S. Hanada, O. Izumi, *ISIJ Int.* 31 (1991) 807–813.
- [8] M.F. Ijaz, H.Y. Kim, H. Hosoda, S. Miyazaki, *Scripta Mater.* 72–73 (2014) 29–32.
- [9] Y. Al-Zain, Y. Sato, H.Y. Kim, H. Hosoda, T.H. Nam, S. Miyazaki, *Acta Mater.* 60 (2012) 2437–2447.
- [10] S. Cai, J.E. Schaffer, Y. Ren, *Mater Sci Eng A* 680 (2017) 13–20.
- [11] E. Takahashi, T. Sakurai, S. Watanabe, N. Masahashi, S. Hanada, *Mater. Trans.* 43 (2002) 2978–2983.
- [12] Y.L. Hao, S.J. Li, S.Y. Sun, R. Yang, *Mater Sci Eng A* 441 (2006) 112–118.
- [13] S. Cai, J.E. Schaffer, Y. Ren, *Mater. Res. Lett.* 4 (2016) 161–167.
- [14] Y.L. Hao, S.J. Li, S.Y. Sun, C.Y. Zheng, Q.M. Hu, R. Yang, *APL* 87 (2005), 091906.
- [15] J.C. Williams, B.S. Hickman, D.H. Leslie, *Metall. Trans.* 2 (1971) 477–484.
- [16] S. Hanada, C. Izumi, *Metall. Trans.* 18 (1987) 265–271.
- [17] Masahiko Ikeda, Shin-ya Komatsu, Yuichiro Nakamura, *Mater. Trans.* 45 (2004) 1106–1112.
- [18] H. Matsumoto, S. Watanabe, S. Hanada, *J. Alloys Compd.* 439 (2007) 146–155.
- [19] H. Matsumoto, S. Watanabe, S. Hanada, *Mater. Trans.* 46 (2005) 1070–1078.
- [20] M.F. Ijaz, H.Y. Kim, H. Hosoda, S. Miyazaki, *Mater. Sci. Eng. C* 48 (2015) 11–20.
- [21] B.L. Wang, Y.F. Zheng, L.C. Zhao, *Mater Sci Eng A* 486 (2008) 146–151.
- [22] E. Bertrand, P. Castany, Y. Yang, E. Menou, T. Gloriant, *Acta Mater.* 105 (2016) 94–103.
- [23] Y. Guo, K. Georgarakis, Y. Yokoyama, A.R. Yavari, *J. Alloys Compd.* 571 (2013) 25–30.
- [24] S. Cai, L. Wang, J.E. Schaffer, J. Gao, Y. Ren, *Mater Sci Eng A* 743 (2019) 764–772.
- [25] S. Miyazaki, H.Y. Kim, H. Hosoda, *Mater. Sci. Eng. A* 438–440 (2006) 18–24.
- [26] S. Cai, J.E. Schaffer, Y. Ren, *APL* 106 (2015) 131907.
- [27] J.I. Kim, H.Y. Kim, T. Inamura, H. Hosoda, S. Miyazaki, *Mater Sci Eng A* 403 (2005) 334–339.
- [28] P.J.S. Buenconsejo, H.Y. Kim, S. Miyazaki, *Acta Mater.* 57 (2009) 2509–2515.
- [29] J.C. Williams, B.S. Hickman, D.H. Leslie, *Metall. Trans.* 2 (1971) 477–484.
- [30] Y. Okazaki, Y. Ito, A. Ito, T. Tateishi, in: S.A. Brown, J.E. Lemons (Eds.), *Medical Applications of Titanium and its Alloys: the Material and Biological Issues*, ASTM STP 1272, ASTM, 1996, pp. 45–59.
- [31] H.Y. Kim, S. Miyazaki, *Shap. Mem. Superelasticity* 2 (2016) 380–390.
- [32] M.F. Ijaz, H.Y. Kim, H. Hosoda, S. Miyazaki, *Mater. Sci. Eng. C* 48 (2015) 11–20.
- [33] A.P. Hammersley, *FIT2D V9.129 Reference Manual V3.1*, ESRF Internal Report, 1998.
- [34] H.M. Rietveld, *J. Appl. Crystallogr.* 2 (1969) 65–71.
- [35] L. Lutterotti, S. Matthies, H.-R. Wenk, A.S. Schulz, J.W. Richardson Jr., *J. Appl. Phys.* 81 (1997) 594.
- [36] S. Cai, M.R. Daymond, Y. Ren, J.E. Schaffer, *Acta Mater.* 61 (2013) 6830–6842.
- [37] C. Baker, *Met. Sci. J* 5 (1971) 92–100.
- [38] D.R.N. Correa, F.B. Vicente, T.A.G. Donato, V.E. Arana-Chavez, M.A.R. Buzalaf, C. R. Grandini, *Mater. Sci. Eng. C* 34 (2014) 354–359.
- [39] I.L. Dillamor, W.T. Roberts, *Metall. Rev.* 10 (1965) 271–380.
- [40] M. Tahara, H.Y. Kim, H. Hosoda, S. Miyazaki, *Acta Mater.* 57 (2009) 2461–2469.
- [41] S. Miyazaki, Y. Igo, K. Otsuka, *Acta Metall.* 34 (1986) 2045–2051.
- [42] H. Tada, T. Yamamoto, X. Wang, H. Kato, *Mater. Trans.* 54 (2013) 1502–1509.